Nonequilibrium variational cluster perturbation theory: Quench dynamics of the quantum Ising model

Mohammad Zhian Asadzadeh,[1,2] Michele Fabrizio,[2] and Enrico Arrigoni[1]
[1]*Institute of Theoretical and Computational Physics, Graz University of Technology, 8010 Graz, Austria*
[2]*International School for Advanced Studies (SISSA), Via Bonomea 265, 34136 Trieste, Italy*
(Received 3 May 2016; revised manuscript received 29 October 2016; published 28 November 2016)

We introduce a variational implementation of cluster perturbation theory (CPT) to address the dynamics of spin systems driven out of equilibrium. We benchmark the method with the quantum Ising model subject to a sudden quench of the transverse magnetic field across the transition or within a phase. We treat both the one-dimensional case, for which an exact solution is available, as well the two-dimensional case, for which we have to resort to numerical results. Comparison with exact results shows that the approach provides a quite accurate description of the real-time dynamics up to a characteristic timescale τ that increases with the size of the cluster used for CPT. In addition, and not surprisingly, τ is small for quenches across the equilibrium phase transition point, but can be quite larger for quenches within the ordered or disordered phases.

DOI: 10.1103/PhysRevB.94.205146

I. INTRODUCTION

The remarkable progresses of experiments on ultracold atoms trapped in optical lattices [1–3] have boosted a great interest in the nonequilibrium dynamics of closed quantum systems, especially when they are suddenly pushed across a quantum critical point [4,5]. A rich theoretical activity thus flourished, starting from the paradigmatic example of quantum criticality; namely, the quantum Ising model [6–8].

Developing suitable tools for handling many-body systems out of equilibrium is a big challenge that started some time ago with the pioneering works by Kubo [9], Schwinger [10], Kadanoff and Baym [11], and Keldysh [12]. This effort continued with the work by Wagner [13], who unified the Feynman, Matsubara, and Keldysh perturbation theories into a single and very flexible formalism, until the latest developments related to dynamical mean field and related cluster-embedding methods (see, e.g., Refs. [14–25]). We shall in particular be concerned with the very recent out-of-equilibrium generalization of cluster perturbation theory (CPT) [26,27], which is attractive and conceptually simple [21]. In CPT the lattice is divided into small clusters which can be diagonalized exactly. The intercluster terms are then treated within strong-coupling perturbation theory. Its nonequilibrium version allows us to investigate the unitary quantum evolution in the thermodynamic limit, accounting for nonlocal correlations on a length scale defined by the size of the considered cluster. Besides the simplicity of the formulation, the efficiency and accuracy of the specific implementation is also of major importance.

The main purpose of this work is to develop a nonequilibrium variational implementation of CPT for spin systems. We test the method on the quantum Ising model after a sudden quench of the transverse field. Since the model is exactly solvable in one dimension we have the possibility to benchmark the approach. We also investigate the same model in two dimensions where an exact solution is not available. In this case, we compare with finite-size exact diagonalization results. We discuss in detail how to efficiently implement the method to allow reaching relatively long simulation times with moderate computational effort.

The paper is organized as follows: In Sec. II the nonequilibrium Green's function formalism is briefly presented. The model we study is introduced in Sec. III. Section IV describes the CPT method together with its self-consistent variational improvement. Results are reported in Sec. V. Section VI is devoted to concluding remarks.

II. NONEQUILIBRIUM GREEN'S FUNCTIONS

In this section we briefly outline the nonequilibrium Green's function formalism to set up the notations that we shall use throughout the paper. There is a wide literature on the subject but in this work we mainly follow the Kadanoff–Baym–Wagner scheme [11,13].

Consider a system initially (at time $t_0 = 0$) at equilibrium and described by a Hamiltonian H_{eq} and temperature $1/\beta$. At $t > t_0$, a generic time-dependent Hamiltonian $H(t)$ is switched on. The nonequilibrium formalism works through averages of time-ordered products of operators along the Kadanoff–Baym contour [11,12,28,29] shown in Fig. 1. The contour is composed of three branches: it starts at $t_0 = 0$, runs up to $t_{\max}$ and then back to the initial time, and finally moves parallel to the imaginary axis up to $\tau = -i\beta$. Due to the lack of time translation invariance, the nonequilibrium single-particle Green's function depends on two time variables rather than on their difference and is defined as the contour-ordered expectation value

$$\begin{aligned} G_{i,j}(z,z') &= -i\langle \mathcal{T}_{\mathcal{C}} a_i(z) a_j^\dagger(z')\rangle \\ &= -i\theta^{\mathcal{C}}(z-z')\langle a_i(z)a_j^\dagger(z')\rangle \\ &\quad - i\theta^{\mathcal{C}}(z'-z)\langle a_j^\dagger(z')a_i(z)\rangle, \end{aligned} \tag{1}$$

where $a_i^\dagger$ (a_i) are the creation (annihilation) operators for particles, in the present case bosons, at site i and z, z' are variables on the contour $\mathcal{C}$ and can be real or imaginary depending on the branch of the contour in which they lie. The time evolution of the operators on the Kadanoff–Baym contour is defined in the Heisenberg picture with Hamiltonian $H(z)$. $\mathcal{T}$ is the time-ordering operator and is defined via the contour step function $\theta^{\mathcal{C}}(z-z')$. The averages in Eq. (1) are

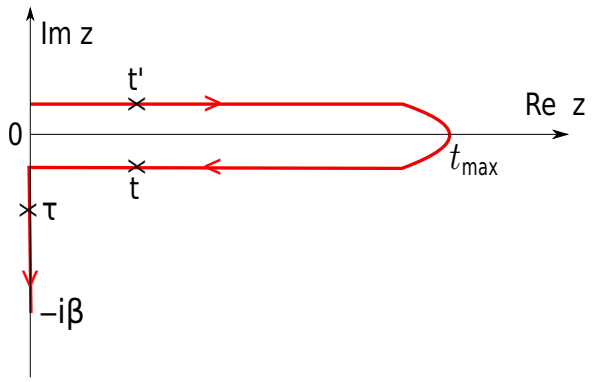

FIG. 1. The L-shaped Kadanoff–Baym contour $\mathcal{C}$. The arrows indicate the contour ordering. For example, t' lies ahead of t in the ordering ($t > t'$), i.e., operators at t' are sorted to the right by the contour ordering.

over the initial equilibrium Hamiltonian $H_{\rm eq}$ at temperature $1/\beta$.

The Dyson equation reads

$$\hat{G} = \hat{G}_0 + \hat{G}_0 \bullet \hat{\Sigma} \bullet \hat{G}, \tag{2}$$

where $\hat{G}_0$ is the bare Green's function and $\hat{\Sigma}$ is the self-energy. The product symbol $\bullet$ denotes the matrix multiplication in space and the integration over the time variables along the contour $\mathcal{C}$.

For a given Green's function $\hat{G}(z,z')$ each variable z,z' can lay on one of the three branches of the contour in Fig. 1. This prompts an alternative representation of $\hat{G}$ as a 3×3 matrix, as introduced by Wagner [13]. Of the 9 matrix elements, only 6 are linearly independent, so that after a suitable transformation one is left with 6 nonzero terms, which are referred to as the retarded (G^R), advanced (G^A), Keldysh (G^K), left-mixing ($G^{\rceil}$), right-mixing ($G^{\lceil}$), and Matsubara Green's function (G^M). They are explicitly given as

$$\begin{aligned}
G^R_{i,j}(t,t') &= -i\theta(t-t')\langle[a_i(t),a_j^\dagger(t')]\rangle,\\
G^A_{i,j}(t,t') &= G^R_{j,i}(t',t)^*,\\
G^K_{i,j}(t,t') &= -i\langle\{a_i(t),a_j^\dagger(t')\}\rangle,\\
G^{\rceil}_{i,j}(t,\tau) &= -i\langle a_j^\dagger(\tau)a_i(t)\rangle,\\
G^{\lceil}_{i,j}(\tau,t) &= -i\langle a_i(\tau)a_j^\dagger(t)\rangle,\\
G^M_{i,j}(\tau,\tau') &= -\langle\mathcal{T}_\tau a_i(\tau)a_j(\tau')\rangle,
\end{aligned} \tag{3}$$

where t and t' are real times and $\tau,\tau' \in [0,-i\beta]$. In the above equations $\{\dots\}$ and $[\dots]$ stand for anticommutator and commutator, respectively.

III. HAMILTONIAN

The Hamiltonian of the Ising model in a transverse field is given by

$$H = -J\sum_{\langle i,j\rangle} S_i^x S_j^x + h\sum_i S_i^z, \tag{4}$$

where $\langle i,j\rangle$ means summation over nearest-neighbor spins, and h is the strength of the magnetic field, with $J > 0$ and $h > 0$. In the following we shall work in units of $J = 1$. The Hamiltonian of Eq. (4) in one dimension has an exact solution which is obtained by a Jordan–Wigner transformation that maps the system onto a quadratic Hamiltonian for spinless fermions, which can be exactly solved [30,31]. On the other hand, in two dimensions an exact solution is not available [32].

Cluster embedded techniques such as CPT in equilibrium have been applied to fermionic and bosonic systems [33–37]. Out of equilibrium, CPT has been applied to the fermionic Hubbard model [21,22]. Here we formulate nonequilibrium CPT for spin systems, exploiting the well-known equivalence between spin-$\frac{1}{2}$ operators are hard-core bosons. We also provide a variational improvement of it, which allows us to treat the ordered phase.

Specifically, if we assume that spin-up corresponds to the presence of a hard-core boson, and spin-down to its absence, the following relationships between spin and boson operators hold [4]:

$$\begin{aligned}
S^+ &\to a^\dagger,\\
S^- &\to a,\\
S^z &\to a^\dagger a - \tfrac{1}{2},\\
S^x &\to (a + a^\dagger)/2,
\end{aligned} \tag{5}$$

where S^+ and S^- are the raising and lowering spin operators, respectively.

The Hamiltonian in the bosonic representation then becomes

$$\begin{aligned}
H = &-\frac{J}{4}\sum_{\langle i,j\rangle}(a_i a_j + a_i^\dagger a_j^\dagger + a_i a_j^\dagger + a_i^\dagger a_j)\\
&+ h\sum_i\left(a_i^\dagger a_i - \frac{1}{2}\right) + U\sum_i n_i(n_i-1),
\end{aligned} \tag{6}$$

where the on-site Hubbard-like term enforces the hard-core constraint when $U \to \infty$, and $n_i = a_i^\dagger a_i$. Since the Hamiltonian contains also anomalous terms like $a_i^\dagger a_j^\dagger$ and $a_i a_j$ the Green's function matrix $\hat{G}$ of Eq. (2) contains anomalous Green's functions F and $F^\dagger$ as follows:

$$\begin{aligned}
F_{i,j}(z,z') &= -i\langle\mathcal{T}_\mathcal{C} a_i(z)a_j(z')\rangle,\\
F^\dagger_{i,j}(z,z') &= -i\langle\mathcal{T}_\mathcal{C} a_i^\dagger(z)a_j^\dagger(z')\rangle,
\end{aligned} \tag{7}$$

where variables z, z' can lie on one of three branches of the contour in Fig. 1.

IV. METHOD

A. Cluster perturbation theory

Cluster perturbation theory (CPT) [26,27] is a simple quantum cluster method to deal with correlated systems. In this approach the idea is to embed a finite cluster of sites, for which a numerically exact solution is affordable, into the infinite lattice. In practice the starting point is to partition the original D-dimensional lattice of linear size L into clusters of linear size L_c with open boundaries. Figure 2 shows an example for a tiling in $D = 1$ and $L_c = 4$. All clusters are considered as supercells that form a superlattice, each supercell

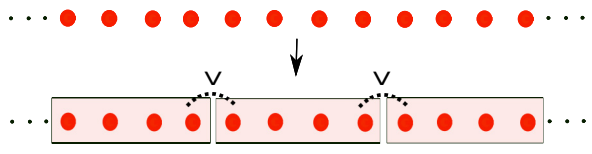

FIG. 2. Partitioning of a $D = 1$ lattice into clusters with size $L_c = 4$. The intercluster hopping is denoted by V.

being identified by a superlattice vector r. The sites within each cluster are in turn labeled by vectors R. The lattice Hamiltonian H is thus written as

$$H = H_0 + V, \tag{8}$$

where H_0 corresponds to the cluster Hamiltonian and V describes the intercluster terms. CPT Green's function can be obtained by a subsequent expansion in powers of the intercluster hopping. Diagrammatic [38,39] and cluster dual fermion approaches [40] provide a systematic expansion in terms of the intercluster terms, which then has to be truncated at some order. Within strong-coupling perturbation theory [26,41] one obtains an expression for the lattice Green's function at lowest order:

$$G(\omega) = G_0(\omega) - G_0(\omega) V G(\omega), \tag{9}$$

where V is the matrix representation of the intercluster hopping, $G_0(\omega)$ is the exact equilibrium Green's function of the cluster, and the product is just a matrix multiplication in lattice sites. The Green's function G_0 is diagonal in r and identical for all supercells, whereas V is off-diagonal in r. Because of superlattice translation invariance, the above equation is simpler in momentum space. After partial Fourier transform, $r \to q$, the CPT equation transforms into

$$G(q,\omega) = G_0(\omega) - G_0(\omega) V(q) G(q,\omega), \tag{10}$$

where now G, G_0, and V are matrices in the label R of the sites within each supercell. The CPT is a conceptually simple method that nevertheless includes short-range correlations on the scale of cluster size and therefore requires moderate computational resources.

The idea of CPT can be straightforwardly transferred to the nonequilibrium situation by replacing the equilibrium frequency-dependent Green's functions with the contour-ordered ones. The authors of Ref. [21] have developed a nonequilibrium formulation for CPT (NE-CPT) and examined how the technique works for the Fermi–Hubbard model. The NE-CPT equation reads as follows:

$$\hat{G}(q) = \hat{G}_0 + \hat{G}_0 \bullet \hat{V}(q) \bullet \hat{G}(q). \tag{11}$$

The solution of Eq. (11) provides the nonequilibrium CPT Green's function $\hat{G}(q)$. In the NE-CPT equation the product symbol $\bullet$ denotes not only the matrix multiplication but also an integration over time variables along the contour $\mathcal{C}$. Furthermore, $\hat{V}(q) = V(q) \bigotimes \mathbb{1}$ where $\mathbb{1}$ is a δ function on the contour, i.e., $\delta(z' - z) = \mathbb{1}$. In what follows we omit the momentum dependence to simplify notations. The explicit integral form of Eq. (11) is

$$\hat{G}(z,z') = \hat{G}_0(z,z') + \int_{\mathcal{C}} dz_1 \hat{G}_0(z,z_1) V \hat{G}(z_1,z'), \tag{12}$$

where integration is carried out along the three branches of the contour $\mathcal{C}$ in Fig. 1, i.e.,

$$\int_{\mathcal{C}} dz_1 = \int_0^{t_{\max}} dt - \int_0^{t_{\max}} dt + \int_0^{-i\beta} d\tau. \tag{13}$$

The numerical solution of the generic contour equation (12) requires discretization of the time variable. A straightforward but not efficient solution for $\hat{G}$ involves a matrix inversion [21] where large matrices in discretized time are used. In this manner reaching long time dynamics is computationally prohibitive. Alternatively, by using the Kadanoff–Baym equations [11,42] one can derive the same integral equation (12) for the components of $\hat{G}$ in the Wagner representation [see Eq. (3)]. A practical application of this approach to nonequilibrium dynamical mean-field theory (NE-DMFT) has been presented by Tran [43]. This method takes advantage of the causality of the integral equations: the properties of the system at specific time $t = t_1$ do not depend on the information at $t > t_1$ and so its *a priori* knowledge is not required in the calculation. Here we follow this approach but for spatially inhomogeneous systems. For details of the procedure and technical issues see Appendix A.

B. Variational cluster perturbation theory

Within CPT one is free to add an arbitrary single-particle term $-\Delta$ to the cluster Hamiltonian H_0 [Eq. (8)] provided that it is then subtracted perturbatively, i.e., added to V, such that the Hamiltonian H remains unchanged. The CPT expansion is now carried out in the new perturbation $\bar{V} = V + \Delta$ with the new cluster Hamiltonian $H' = H_0 - \Delta$. While ideal exact results should not depend on Δ, in practice results do depend on Δ due to the approximate nature of the CPT expansion.

In this work we shall consider a Z_2 symmetry-breaking term:

$$\Delta = \sum_{R=1}^{L_c} f_R S_R^x = \sum_{R=1}^{L_c} \frac{f_R}{2} (a_R + a_R^\dagger), \tag{14}$$

where f_R are real variational parameters to be fixed. We remind the reader that a_i ($a_i^\dagger$) are bosonic operators with hard-core constraint [see Eq. (5)]. We show below that accounting for this variational term is crucial to describe the ordered phase of the quantum Ising model. The optimum value of the variational parameters f_R should be determined through a variational principle [16,44,45]. Here we shall resort to a simplified version of the variational procedure introduced in Refs. [44,45]. Specifically, we fix the variational parameters within a self-consistent approach where the intercluster term $S_i^x S_j^x$ is replaced with its mean-field approximation as

$$S_i^x S_j^x = \langle S_i^x \rangle S_j^x + S_i^x \langle S_j^x \rangle - \langle S_i^x \rangle \langle S_j^x \rangle. \tag{15}$$

In one dimension, for example, upon tiling the infinite lattice into clusters of size L_c, the mean-field expression for the supercell Hamiltonian at equilibrium is

$$H' = -J \sum_{R=1}^{L_c - 1} S_R^x S_{R+1}^x + h_0 \sum_{R=1}^{L_c} S_R^z - f_{L_c} S_1^x - f_1 S_{L_c}^x, \tag{16}$$

where $f_R = J\langle S^x_R\rangle$, $R = 1$, L_c are the mean-field self-consistency conditions and, by reflection symmetry, we shall set $f_1 = f_{L_c}$. The procedure to find parameter f_R is as follows: We start with a guess for variational parameter and then, after plugging them in the cluster Hamiltonian of Eq. (16), the new f_R is calculated as $f_R = J\langle S^x_R\rangle$. The new f_R is used for the next iteration and the loop will be terminated when the difference between new and old f_R is less than the required accuracy.

Out of equilibrium the variational parameters become time dependent. The protocol we shall implement is a sudden quench of the magnetic field from h_0 to a different value h. Therefore, the explicit time-dependent mean-field cluster Hamiltonian becomes

$$H'(t) = -J\sum_{R=1}^{L_c-1} S^x_R S^x_{R+1} + h\sum_{R=1}^{L_c} S^z_R - f_{L_c}(t)S^x_1 - f_1(t)S^x_{L_c}, \tag{17}$$

with the self-consistency condition

$$f_R(t) = f_R(t)^* = J\langle\Psi(t)\big|S^x_R\big|\Psi(t)\rangle, \tag{18}$$

where $|\Psi(t)\rangle$ is the time-evolved cluster wave function. To evaluate the time-dependent variational parameters $f_R(t)$, we expand the latter to linear order:

$$|\Psi(t+\Delta t)\rangle \approx [1 - iH'(t)\Delta t]|\Psi(t)\rangle + O(\Delta t^2), \tag{19}$$

starting from the initial equilibrium state $|\Psi(t = t_0)\rangle$. As a result, the parameters $f_i(t+\Delta t)$ can be taken as

$$f_i(t+\Delta t) \approx J\langle\Psi(t)|[1+iH'(t)\Delta t]S^x_i[1-iH'(t)\Delta t]|\Psi(t)\rangle \tag{20}$$

at each time step.

C. Cluster perturbation theory corrections to order parameter

Due to the presence of anomalous terms linear in creation and annihilation operators the new perturbation $\bar{V}$ including Δ [Eq. (14)] is not quadratic in the boson operators and therefore one has to generalize CPT to deal with anomalous terms. The way to do this (see Refs. [44,45]) is to first perform standard CPT on top of the cluster Hamiltonian H' [Eq. (16)] by using just the quadratic part of V as a perturbation. The CPT correction to the condensate can be then obtained by using an expression derived within a so-called pseudoparticle formulation of CPT. This approach is being applied to the Bose–Hubbard model in the superfluid phase and subsequently confirmed more formally within a self-energy functional approach [45]. For the equilibrium case, one obtains

$$G^{-1}\langle A\rangle = G'^{-1}\langle A\rangle' + F, \tag{21}$$

where G and $\langle A\rangle$ are the CPT-corrected Green's function and expectation value of the condensate, respectively, while the terms with primes stands for their cluster values. The vector F describes the variational parameters f of Eq. (14). In Eq. (21) the Green's functions are $2L_c \times 2L_c$ Nambu matrices and the $\langle A\rangle$, $\langle A\rangle'$, and F are $2L_c$ Nambu vectors; namely,

$$\langle A\rangle' = \begin{bmatrix} \langle a'_1\rangle \\ \vdots \\ \langle a'_{L_c}\rangle \\ \langle a'^{\dagger}_1\rangle \\ \vdots \\ \langle a'^{\dagger}_{L_c}\rangle \end{bmatrix}, \quad \langle A\rangle = \begin{bmatrix} \langle a_1\rangle \\ \vdots \\ \langle a_{L_c}\rangle \\ \langle a^{\dagger}_1\rangle \\ \vdots \\ \langle a^{\dagger}_{L_c}\rangle \end{bmatrix}, \quad 2F = \begin{bmatrix} f_1 \\ \vdots \\ f_{L_c} \\ f^*_1 \\ \vdots \\ f^*_{L_c} \end{bmatrix}. \tag{22}$$

Out of equilibrium it is straightforward to generalize Eq. (21) to an equation along the contour:

$$\hat{G}^{-1}\bullet\hat{A} = \hat{G}'^{-1}\bullet\hat{A}' + \hat{F}, \tag{23}$$

where the ingredients are now contour functions. Again, the symbol $\bullet$ represents matrix multiplication in space and time integration along the contour. We further simplify this expression by multiplying both sides of it by $\hat{G}$ from the left. This leads to

$$\hat{A} = \hat{G}\bullet\hat{G}'^{-1}\bullet\hat{A}' + \hat{G}\bullet\hat{F}, \tag{24}$$

where we have used the fact that $\hat{G}\bullet\hat{G}^{-1} = \mathbb{1}$. Via the CPT equation (11) one can further derive the expression

$$\hat{G}\bullet\hat{G}'^{-1} = \mathbb{1} + \hat{G}\bullet\hat{V}. \tag{25}$$

After substituting into Eq. (24), one finally gets the following equation for the condensate including the CPT correction:

$$\hat{A} = \hat{A}' + \hat{G}\bullet\hat{V}\bullet\hat{A}' + \hat{G}\bullet\hat{F}. \tag{26}$$

We rewrite this equation by expressing the contour integration explicitly as

$$\hat{A}(z) = \hat{A}'(z) + \int_c d\bar{z}\hat{G}(z,\bar{z})[V\hat{A}'(\bar{z}) + \hat{F}(\bar{z})], \tag{27}$$

where $z, \bar{z}$ are contour variables (see Fig. 1). By employing Langreth theorem [46] one can break down the contour integrations into contributions on the real and imaginary time axes. For the condensate on the real time branch of the contour we get

$$A(t) = A'(t) + \int_0^t d\bar{t}G^R(t,\bar{t})[VA'(\bar{t}) + F(\bar{t})] + \int_0^{-i\beta} d\bar{\tau}G^{\rceil}(t,\bar{\tau})[VA'(\bar{\tau}) + F(\bar{\tau})], \tag{28}$$

where we have used $G^R(t,t') = \theta(t-t')[G^>(t,t') - G^<(t,t')]$. Similarly for the condensate on the Matsubara branch we derive

$$A(\tau) = A'(\tau) + \int_0^{-i\beta} d\bar{\tau}G^M(\tau,\bar{\tau})[VA'(\bar{\tau}) + F(\bar{\tau})]. \tag{29}$$

We note from Eq. (28) that, in order to evaluate $A(t)$ within CPT, the mixing Green's function $G^{\rceil}$ and retarded Green's function G^R have to be determined first. It is crucial to employ high-order numerical integration schemes to accurately simulate up to long times. We refer to Appendix A for more details.

D. Magnetization

The time-dependent magnetization is obtained as

$$S^z(t) = \frac{1}{L}\sum_q \sum_{R=1}^{L_c} \left\langle a^\dagger_{R,q}(t)a_{R,q}(t) - \frac{1}{2}\right\rangle, \quad (30)$$

where $L = N_c L_c$ is the total size of the lattice. The occupation is

$$\langle a^\dagger_{R,q}(t)a_{R,q}(t)\rangle = \langle a^\dagger_{R,q}(t)a_{R,q}(t)\rangle_c + \langle a^\dagger_{R,q}(t)\rangle\langle a_{R,q}(t)\rangle, \quad (31)$$

where the connected part comes from the lesser component of the Green's function within CPT:

$$\langle a^\dagger_{R,q}(t)a_{R,q}(t)\rangle_c = iG^<_{RR,q}(t,t), \quad (32)$$

and the second term is the contribution from the condensate which is the same for all the clusters.

The final expression for the magnetization reads

$$S^z(t) = \frac{1}{L}\sum_q\sum_R iG^<_{RR,q}(t,t) + \frac{1}{L_c}\sum_{R=1}^{L_c}\left(\langle a^\dagger_R(t)\rangle\langle a_R(t)\rangle - \frac{1}{2}\right), \quad (33)$$

where $\langle a^\dagger_R(t)\rangle$ and $\langle a_R(t)\rangle$ are elements of the vector $A(t)$; see Eq. (28).

For a finite lattice with open boundary conditions, translation symmetry is lost and therefore the magnetization is position dependent, more pronounced close to the boundaries.

V. RESULTS

In the following we apply the technique discussed in the previous section for both equilibrium and nonequilibrium situations. Moreover, by comparing the results with exact ones in one dimension we assess the accuracy of the method.

A. Equilibrium results

Before applying the technique out of equilibrium we investigate its ability to describe the system already in equilibrium. This is actually a necessary step since the present nonequilibrium protocol assumes that the system is prepared as the ground state of an initial Hamiltonian and is then evolved with a different Hamiltonian. Therefore, an accurate equilibrium state is a prerequisite for getting a sensible after-quench dynamics. The CPT method can work directly in the thermodynamic limit; however, to compare with exact results in one dimension, we consider a finite system with linear size $L = 8$ with open boundary conditions. In the CPT method the procedure is thus to divide the system into two parts, A and B, each one with size $L_c = 4$, and then treat the intercluster term perturbatively; see Fig. 2.

We first set the anomalous term to zero in the cluster Hamiltonian, i.e., $\Delta = 0$ in Eq. (14). In Fig. 3 we display the magnetization parallel to the magnetic field, $\langle S^z\rangle$, for sites $i = 1$ to $i = 4$ compared with the exact result. As we see, CPT works well for large values of magnetic field and reproduces results close to exact results. By contrast, upon decreasing h the accuracy decreases. Standard CPT totally fails close to the mean-field critical field ($h_c = 0.7$). Therefore, the standard CPT is unable to correctly describe the physics for $h < 0.7$.

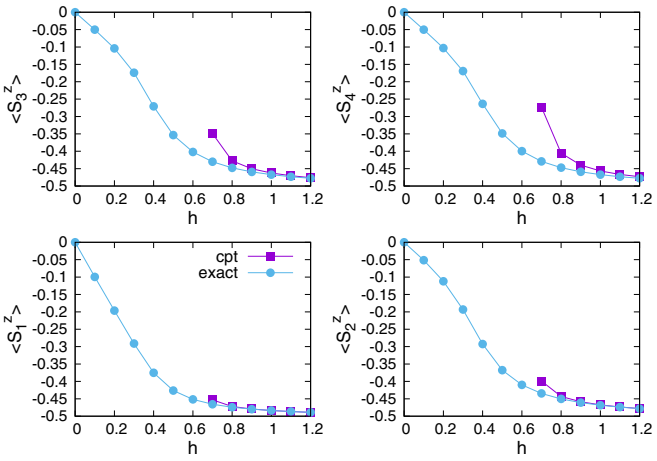

FIG. 3. Magnetization along the z direction versus magnetic field for different sites on a lattice of size $L = 8$ with open boundary conditions. Cluster size in CPT is $L_c = 4$. Exact results are also being reported for comparison.

This kind of instability is well known in approaches based on the bosonic Bogoliubov approximation, such as the spin-wave approximation. The Green's function for free bosons [$U = 0$ in the Hamiltonian of Eq. (6)] has two poles at $z = \pm(h^2 - \frac{J^2}{4})^{1/2}$. It is clear that, for $h < J/2$, the poles move to the imaginary axis, a clear signal of an instability. The same explanation applies to the interacting Hamiltonian (6) and to the instability seen in Fig. 3. The poles of the Green's function become complex for small values of magnetic field, i.e., for $h < 0.7$. This is the region where the hard-core constraint of the bosons becomes important and the standard CPT fails to satisfy this condition. We control the location of the poles by adding the variational term Δ in Eq. (14) to the cluster Hamiltonian, which explicitly breaks the Z_2 symmetry and induces the spontaneous breaking of such symmetry at low fields. After finding self-consistently the optimum value for the variational parameters we compute the CPT corrections as explained in the previous section.

In Fig. 4 in the left panel we show the variational CPT (VCPT) result for the ground-state energy compared with the exact one. The agreement is quite good in the whole range of magnetic fields. On the other hand, it is well known that the energy is a quantity that is not very sensitive to perturbations, so one could argue that this agreement is not significant. On the other hand, the right panel shows the value of the variational parameter $f = J\langle S^x_{1B}\rangle = J\langle S^x_{4A}\rangle$. This quantity shows a phase transition at $h_c = 0.7$, below which $\langle S^x\rangle$ acquires a finite value. Strictly speaking, such a phase transition should not occur in a finite-size system, where $\langle S^x\rangle$ must be zero by symmetry, so its emergence is a spurious results that derives from the variational scheme. In the thermodynamic limit the transition does occur instead, although the critical field is known to be $h_c = 0.5$. Nevertheless, by increasing the length L_c of the cluster up to $L_c = 16$ we observe a decrease of h_c to values close to the exact value. For the time-dependent calculation and for our benchmark, however, we have to stick to smaller

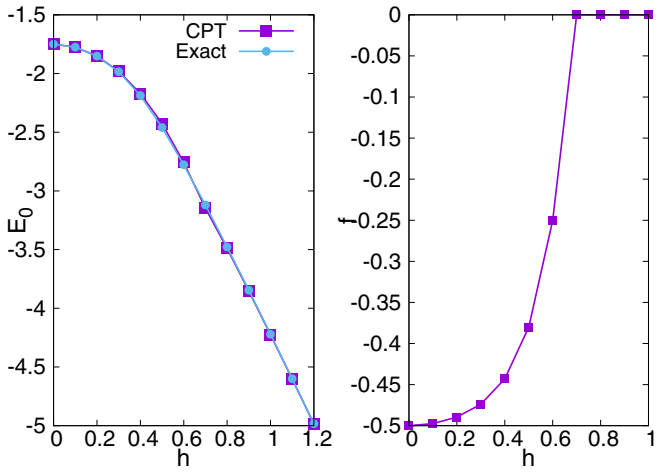

FIG. 4. (left panel) Ground-state energy from VCPT compared with the exact value for lattice of size $L = 8$ with open boundary conditions. (right panel) $f = J\langle S^x_{1B}\rangle = J\langle S^x_{4A}\rangle$.

values of $L_c = 4$. Keeping in mind this caveat, let us turn to compare other physical observables different from S^x.

In Fig. 5 we report the z magnetization on the sites 1,2,3,4 compared with the exact value. As we see, the comparison is quite satisfactory. At site $i = 1$ and for the whole range of magnetic fields, VCPT results are very close to exact results, especially in the instability region $h \leqslant 0.5$. Around $h = 0.7$ the results are less close to the exact ones, mainly for the site $i = 4$ at the edge of the system.

It is worth mentioning that the hard-core constraint implies the following relation between expectation values:

$$\langle a_i^\dagger a_i\rangle + \langle a_i a_i^\dagger\rangle = 1. \tag{34}$$

We found that, within the present self-consistent VCPT, the expectation value of the above expression slightly deviates from unity by about 10^{-3} on the average, with a maximum of the order of 10^{-2} at $h = 0.7$ and for the sites at the edge of the supercell, as shown by the kink around $h = 0.7$ in Fig. 5. This is due to the fact that treating intercluster terms perturbatively violates the constraint within VCPT, mainly for the edge sites.

Our investigation of a finite cluster shows that, in an ordered phase where the parameters f_R are nonzero, variational CPT (VCPT) and cluster mean field are very close and VCPT only slightly improves the values of local observables. On the other hand, for large magnetic fields for which $f_R = 0$ the VCPT is preferable since cluster mean field misses the interaction of neighboring clusters. More importantly, within VCPT, it is possible to evaluate intercluster correlations for both finite and infinite systems, while in cluster mean field one is limited to intracluster correlations. Finally, in principle, within VCPT one can always improve the results by considering extra variational parameters in the cluster Hamiltonian.

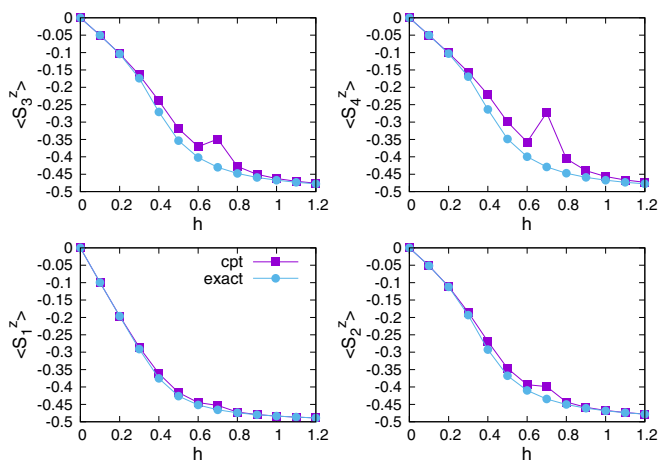

FIG. 5. Magnetization of different sites versus magnetic field for a lattice of size $L = 8$ with open boundary conditions. The cluster size in VCPT is $L_c = 4$. Exact results are also reported for comparison.

B. Nonequilibrium results

In this section we present results for the real time dynamics of the Ising model within the variational cluster perturbation approach introduced above. To drive the system out of equilibrium we proceed as follows: We prepare the system at equilibrium for $t_0 < 0$ as the ground state of Eq. (4) with magnetic field h_0 and then we suddenly change the magnetic field to a different value h. As in equilibrium we use nonequilibrium variational CPT (NE-VCPT) in a self-consistent way as described in Sec. IV. After finding the time-dependent variational parameters for each time step in the mean-field approximation, we calculate the Green's function and condensate within CPT, as described in Sec. IV.

To benchmark this idea for the nonequilibrium case, we display in Fig. 6 the real-time dynamics of magnetization for different sites on a lattice of size $L = 8$ with open boundary conditions at zero temperature. We compare results obtained exactly with results within NE-VCPT for a cluster size of $L_c = 4$. We have reported the dynamics for the case of relatively large quench, from $h_0 = 0.2$ to $h = 1.2$, for which the field crosses the phase transition. As we can see, NE-VCPT provides quite good results for the magnetization compared

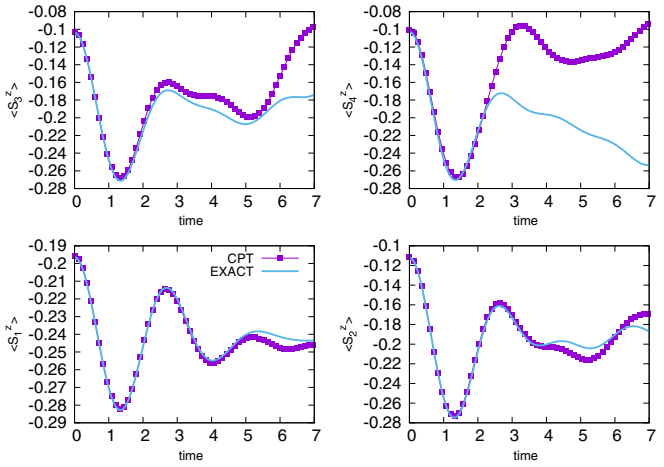

FIG. 6. Time dependence of the magnetization in the z direction for different sites on a lattice of size $L = 8$. The cluster size in NE-VCPT is $L_c = 4$. The magnetic field has been suddenly changed from $h_0 = 0.2$ to $h = 1.2$. The exact dynamics is shown for comparison.

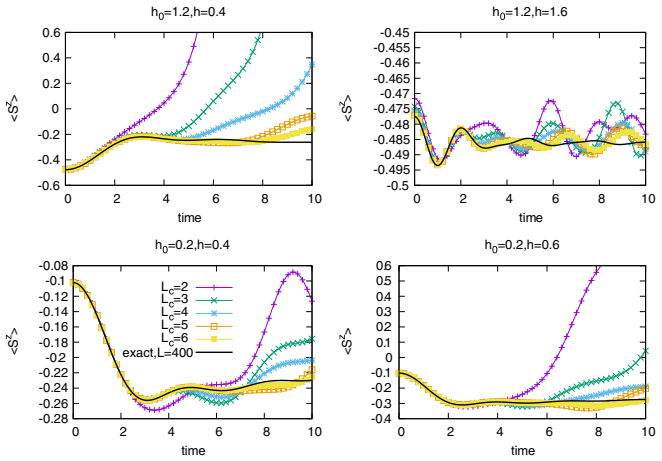

FIG. 7. Time dependence of the magnetization for an infinite Ising chain evaluated within NE-VCPT with different cluster sizes L_c compared with exact results for a chain of length $L = 400$.

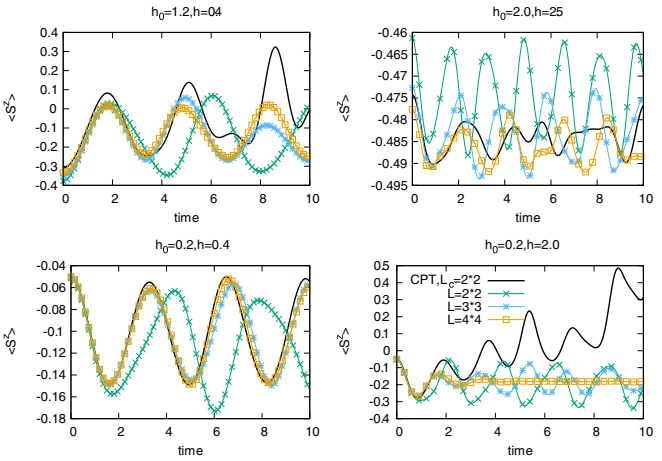

FIG. 8. Dynamics for the magnetization compared with Lanczos results for different types of quenches in two dimension. NE-VCPT calculation is for an infinite lattice with the cluster size of $L_c = 2\times2$.

with the exact one except for the edge sites where the hopping to the next supercell is treated perturbatively. At the beginning of the dynamics NE-VCPT is very accurate and the deviation builds up as time progresses.

We have investigated different types of quenches and the behavior is qualitatively the same: the dynamics remains close to the exact one at short times and starts deviating at later times. As mentioned, the largest deviations are found at the edge sites.

In Fig. 7 we report NE-VCPT results for the magnetization dynamics after the quench for an infinite lattice. We display results obtained for different cluster sizes and different types of quenches. For quenches into the ordered phase (see lower-left and -right panels), NE-VCPT for a cluster of $L_c = 6$ provides quite accurate results for the magnetization dynamics up to $t \approx 7$ (remember that time is in units of $1/J$). For a larger quench from $h_0 = 1.2$ to $h = 0.4$, crossing the transition point, NE-VCPT is able to reproduce the dynamics only up to a shorter value of time $t \approx 5$ (see upper-left panel of Fig. 7). For quenches within the disordered phase (quench from $h_0 = 1.2$ to $h = 1.6$) NE-VCPT results show only a slight deviation ($\lesssim 10^{-3}$) from the exact one; however, with some small oscillations (see upper-right panel of Fig. 7). Overall, NE-VCPT results for an infinite system systematically improve upon increasing cluster size L_c. Already for $L_c = 6$ they reproduce quite accurate results for the thermodynamic limit of a very long chain ($L = 400$) up to $t \approx 7$.

Finally, we report the real-time quench dynamics of the magnetization for the two-dimensional Ising model, which is not exactly solvable. In $D = 2$ the transverse-field Ising model at zero temperature has an equilibrium phase transition at $h_c \approx 1.6$ [47–49]. Within the self-consistent VCPT at equilibrium we get instead $h_c \approx 1.9$, for the small 2×2 clusters we are considering. We note that the accuracy of VCPT improves systematically by increasing cluster size. We show results for different types of quenches which are obtained either within a disordered or a ordered phase or a quench which crosses the critical field. Here, we compare Lanczos exact results obtained for three different lattice sizes with periodic boundary conditions with NE-CPT results by using clusters of size $L_c = 2\times2$. We note that the largest size we can reach to perform real-time quench dynamics within Lanczos at zero temperature is $L = 4\times4$.

For a small quench in the ordered phase, $h_0 = 0.2$ to $h = 0.4$ (Fig. 8, lower-left panel) NE-VCPT gives quite accurate results, as compared with Lanczos exact results. We observe that magnetization dynamics within NE-VCPT is quite close to the best of the Lanczos for times up to $t_{\max} = 10$. We further note that, in this case, the Lanczos results already show convergence as a function of system size so that they can be considered as a good approximation to the thermodynamic limit for these values of the parameters. For a larger quench but still in the ordered phase, i.e., $h_0 = 1.2$ to $h = 0.4$ (top-left panel of Fig. 8) the NE-VCPT results compare well with Lanczos results up to $t_{\max} \approx 6$. For quenches with large magnetic fields, i.e., into the disordered phase from $h_0 = 2.0$ to $h = 2.5$ (top-right panel in Fig. 8) the Lanczos results have not converged yet, so a comparison is difficult to assess. Nevertheless, the NE-VCPT results quantitatively agrees with the largest Lanczos system up to $t \approx 2$, and agrees qualitatively, i.e., displays similar oscillations, also for larger times. The lower-right panel in Fig. 8 shows the dynamics for a large magnetic quench that crosses the critical point, i.e., from $h_0 = 0.2$ to $h = 2.0$. In this case the NE-VCPT seems not to be accurate and is able to produce reliable dynamics only up to $t_{\max} \approx 2$. We note that, in all cases, the magnetization stays within its physical values, $|S^z| \leqslant \frac{1}{2}$, except for a quench across the critical point. With cluster sizes of $L_c = 2\times2$, results are already promising in two dimensions, as long as one remains restricted to intermediate times. Furthermore, as in the $D = 1$ case, NE-VCPT results can be improved by systematically increasing the cluster size.

VI. SUMMARY AND DISCUSSION

We have introduced a variational formulation of cluster perturbation theory (CPT) to investigate the quantum Ising model in and out of equilibrium at zero temperature. We find that plain CPT in equilibrium can describe accurately the

system in the disordered phase, $h > h_c$, but looses accuracy while approaching the critical field h_c and finally breaks down in the ordered phase, $h < h_c$. To describe the system in the broken-symmetry region we developed a variational implementation of CPT (VCPT), whereby an anomalous term is added to the cluster Hamiltonian and subtracted perturbatively. This parameter is then optimized within a self-consistent framework. We find a good agreement with exact results in the equilibrium case; for example, concerning the magnetization parallel to the magnetic field and the ground-state energy.

Out of equilibrium the time-dependent variational parameter are determined self-consistently for each time step. We find that this variational NE-VCPT provides very accurate results for the short- and intermediate-time dynamics while getting inaccurate for longer times. Specifically in one dimension, comparing results of this NE-VCPT approximation with exact calculations shows that clusters of size $L_c = 6$ provide a quite accurate description of the dynamics up to $t_{\max} \approx 7$ for quenches within the ordered or disordered phases. When the critical point is crossed, the accuracy is limited to shorter times $t_{\max} \approx 3$. A similar trend emerges also in two dimensions. Here, there is no exact solution to be compared with, so that we resort to finite-size Lanczos diagonalization to benchmark the method. One should notice, however, that NE-VCPT can directly provide results in the thermodynamic limit. We highlight that the accuracy of NE-VCPT can be systematically pushed to longer time by increasing the cluster size, at least up to the largest sizes still reachable by Lanczos time evolution.

Comparison with other techniques based on matrix product states (MPS) such as time-evolving block decimation (TEBD) [50] and time dependent density-matrix renormalization group (t-DMRG) [51] shows that the present conceptually simple VCPT is performing in a reasonable way, considering the complexity of the implementation of the other algorithms. Within TEBD and t-DMRG, the time dependence of quantum spin models can be achieved quite accurately up to quite large times depending on the initial state of the system [52–56]. These methods are restricted to and work well for one-dimensional gapped systems in which correlation functions decay exponentially and the entanglement has an upper bound. In the cases where entanglement grows in time, the performance of MPS-based methods deteriorate rapidly.

In principle, starting from a given initial state and performing time evolution up to the steady state is computationally expensive or even prohibitive in NE-VCPT, as well as in many other more sophisticated techniques. However, within NE-VCPT one can, alternatively, bypass the transient behavior and directly solve for a time-independent steady state (see, e.g., Ref. [18] for the fermionic case), assuming that one exists. Having done that, one can address the long-time behavior by expanding around the steady state backward in time to obtain results for the relaxation of observables.

This variational approach shall be considered as a first step to study hard-core bosons in and out of equilibrium by a variational CPT method. This idea could be improved and is getting more elaborate by considering more variational terms and/or formulating it within the self-energy functional theory [16].

ACKNOWLEDGMENTS

We would like to thank M. Nuss, M. Aichhorn, and A. Dorda for fruitful discussions. This work was supported by funds awarded by the Friuli Venezia Giulia autonomous Region Operational Program of the European Social Fund 2007/2013, Project DIANET-Danube Initiative and Alps Adriatic Network, CUPG93J12000220009. The work was also partially supported by the Austrian Science Fund (FWF): P26508, Y746, and NaWi Graz.

APPENDIX A: NUMERICAL SOLUTION OF CLUSTER PERTURBATION THEORY EQUATION

1. Time propagation

For spatially inhomogeneous systems, the computational limits are set by the memory requirement for saving big matrices in two time and spatial degrees of freedom. Considering N_K time steps on the Keldysh and N_M on the Matsubara for a lattice of size L the required memory to save the Green's function is

$$[2L(2N_K + N_M)]^2 16 \text{ bytes}. \tag{A1}$$

Therefore, for a $N_K = 1000$, $t_{\max} = 10$, $N_M = 2000$, $\beta = 10$, $L = 8$ the required memory is 61 Gigabytes. This example shows that reaching large time or large system sizes ($t \gtrsim 10J$, $L \gtrsim 6$) is prohibitive since the memory requirement is beyond the capabilities of standard available computational resources. Another issue is the inversion of the huge matrix in the CPT equation to get the lattice Green's function. When the matrix size increases the inversion process takes longer time and also the numerical error will increase.

Based on the above facts one has to design a way to avoid matrix inversion and the storage of huge matrices to finally be able to reach longer times for the dynamics of the system.

2. Procedure to Propagate the Cluster Perturbation Theory Equation in Time

In this section, we summarize the procedure to numerically solve the CPT equation by gradually progressing in time to avoid inversion and storage of big matrices. Since this equation is of the Kadanoff–Baym type, there is a great deal of literature on the subject (see, e.g., Ref. [42]). For example, the method is used in time-dependent dynamical mean-field theory (TDMFT) [19,43], where, however, the system is typically translationally invariant. In our case, where we deal with finite systems, we have to consider spatial degrees of freedom and, accordingly, solve a corresponding set of equations for inhomogeneous systems.

Here, we roughly follow the treatment of Ref. [43]; see also Ref. [42]. In addition, we consider the case of an inhomogeneous system. The CPT equation for the Green's function $\hat{G}$ of the physical system is

$$\hat{G} = \hat{G}_0 + \hat{G}_0 \bullet \hat{V} \bullet \hat{G}, \tag{A2}$$

where $\hat{G}_0$ is the cluster Green's function and $\hat{V} = V \bigotimes \mathbb{1}$ is the intercluster term. By introducing $\hat{K} = \hat{G}_0 \bullet \hat{V}$ we rewrite the CPT equation as

$$\hat{G} = \hat{G}_0 + \hat{K} \bullet \hat{G}, \tag{A3}$$

and, after writing the contour integration explicitly, we have

$$\hat{G}(z,z') = \hat{G}_0(z,z') + \int_{\mathcal{C}} dz_1 \hat{K}(z,z_1)\hat{G}(z_1,z'). \tag{A4}$$

By using the Langreth theorem [46] we can write the integral equation for the components of the Green's function on the contour. We obtain the following equations:

$$\begin{aligned}
G^< &= G_0^< + K^< \cdot G^A + K^R \cdot G^< + K^\rceil * G^\lceil,\\
G^> &= G_0^> + K^> \cdot G^A + K^R \cdot G^> + K^\rceil * G^\lceil,\\
G^R &= G_0^R + K^R \cdot G^R,\\
G^A &= G_0^A + K^A \cdot G^A,\\
G^\rceil &= G_0 + K^R \cdot G^\rceil + K^\rceil * G^M,\\
G^\lceil &= G_0^\lceil + K^\lceil \cdot G^A + K^M * G^\lceil,\\
G^M &= G_0^M + K^M * G^M,
\end{aligned} \tag{A5}$$

where $\cdot$ means integration over real time and $*$ means integration over imaginary time (Matsubara branch).

We are interested in the magnetization which can be calculated from the lesser ($G^<$) Green's function. To solve the equation for $G^<$ first we need to calculate G^A and $G^\lceil$ within CPT. Furthermore, to determine $G^\lceil$ we need to evaluate the Matsubara Green's function G^M which can be calculated with equilibrium techniques. The cluster Green's function G_0^α, ($\alpha = <, R, A, >, \lceil, \rceil$) also should be calculated for an affordable cluster size.

It is also worth to mention that due to the presence of anomalous terms like $a_i a_j$ and $a_i^\dagger a_j^\dagger$ in the Hamiltonian of Eq. (6) the structure of the Green's function matrix also should include anomalous Green's functions in order to satisfy the correct equation of motion. Therefore G^α ($\alpha = <, R, A, >, \lceil, \rceil$) is a matrix in itself with the following Nambu structure:

$$G^\alpha = \begin{bmatrix} g^\alpha & f^\alpha \\ f^{\alpha\dagger} & k^\alpha \end{bmatrix}. \tag{A6}$$

The definition of the Green's functions are as follows:

(1) Advanced Green's function:

$$\begin{aligned}
g_{i,j}^A(t,t') &= i\theta(t'-t)[\langle a_i(t)a_j^\dagger(t')\rangle - \langle a_j^\dagger(t')a_i(t)\rangle],\\
k_{i,j}^A(t,t') &= i\theta(t'-t)[\langle a_i^\dagger(t)a_j(t')\rangle - \langle a_j(t')a_i^\dagger(t)\rangle],\\
f_{i,j}^A(t,t') &= i\theta(t'-t)[\langle a_i(t)a_j(t')\rangle - \langle a_j(t')a_i(t)\rangle],\\
f_{i,j}^{\dagger A}(t,t') &= i\theta(t'-t)[\langle a_i^\dagger(t)a_j^\dagger(t')\rangle - \langle a_j^\dagger(t')a_i^\dagger(t)\rangle].
\end{aligned} \tag{A7}$$

(2) Retarded Green's function:

$$\begin{aligned}
g_{i,j}^R(t,t') &= -i\theta(t-t')[\langle a_i(t)a_j^\dagger(t')\rangle - \langle a_j^\dagger(t')a_i(t)\rangle],\\
k_{i,j}^R(t,t') &= -i\theta(t-t')[\langle a_i^\dagger(t)a_j(t')\rangle - \langle a_j(t')a_i^\dagger(t)\rangle],\\
f_{i,j}^R(t,t') &= -i\theta(t-t')[\langle a_i(t)a_j(t')\rangle - \langle a_j(t')a_i(t)\rangle],\\
f_{i,j}^{\dagger R}(t,t') &= -i\theta(t-t')[\langle a_i^\dagger(t)a_j^\dagger(t')\rangle - \langle a_j^\dagger(t')a_i^\dagger(t)\rangle].
\end{aligned} \tag{A8}$$

There is a relation between retarded and advanced Green's functions: $G^R(t,t') = G^{A\dagger}(t',t)$.

(3) Lesser Green's function:

$$\begin{aligned}
g_{i,j}^<(t,t') &= -i\langle c_j(t')^\dagger c_i(t)\rangle,\\
f_{i,j}^<(t,t') &= -i\langle c_j(t')c_i(t)\rangle,\\
f_{i,j}^{<\dagger}(t,t') &= -i\langle c_j(t')^\dagger c_i(t)^\dagger\rangle,\\
k_{i,j}^<(t,t') &= -i\langle c_j(t')c_i(t)^\dagger\rangle.
\end{aligned} \tag{A9}$$

(4) Mixing Green's function:

$$\begin{aligned}
g_{i,j}^\lceil(\tau,t) &= -i\langle c_i(\tau)c_j^\dagger(t)\rangle,\\
f_{i,j}^\lceil(\tau,t) &= -i\langle c_i(\tau)c_j(t)\rangle,\\
f_{i,j}^{\lceil\dagger}(\tau,t) &= -i\langle c_i^\dagger(\tau)c_j^\dagger(t)\rangle,\\
k_{i,j}^\lceil(\tau,t) &= -i\langle c_i^\dagger(\tau)c_j(t)\rangle,\\
g_{i,j}^\rceil(t,\tau) &= -i\langle c_j(\tau)^\dagger c_i(t)\rangle,\\
f_{i,j}^\rceil(t,\tau) &= -i\langle c_j(\tau)c_i(t)\rangle,\\
f_{i,j}^{\rceil\dagger}(t,\tau) &= -i\langle c_j(\tau)^\dagger c_i(t)^\dagger\rangle,\\
k_{i,j}^\rceil(t,\tau) &= -i\langle c_j(\tau)c_i(t)^\dagger\rangle.
\end{aligned} \tag{A10}$$

If we write the integral equation for G^A we get (omitting the spatial indices):

$$\begin{aligned}
G^A(t,t') &= G_0^A(t,t') + \int K^A(t,\bar{t})G^A(\bar{t},t')d\bar{t},\\
G^A(t,t') &= G_0^A(t,t') + \int_t^{t'} K^A(t,\bar{t})G^A(\bar{t},t')d\bar{t}.
\end{aligned} \tag{A11}$$

To perform the integration, we discretize the time with equal spacing

$$\begin{aligned}
t_i &= i\Delta t + t_0, \quad \Delta t = \frac{t_{\max} - t_0}{N_K - 1} \quad (i = 0,1,\ldots,N_K - 1),\\
\tau_{i'} &= i'\Delta\tau + t_0, \quad \Delta\tau = \frac{-i\beta - t_0}{N_M - 1} \quad (i' = 0,1,\ldots,N_M - 1),
\end{aligned} \tag{A12}$$

where N_K and N_M are the number of time points on the real branch and imaginary branch, respectively. After approximating the integral by the trapezoid rule

$$\int_{t_a}^{t_b} f(x)dx \approx \Delta t \sum_{i=0}^{N-1} \omega_i f(x_i), \quad \Delta t = \frac{t_b - t_a}{N-1},$$

$$w_i = \begin{cases} \frac{1}{2}, & i = 0, N-1 \\ 1, & 1 \leqslant i \leqslant N-2, \end{cases} \tag{A13}$$

we get

$$\begin{aligned}
G^A(t_m,t_n') &\approx G_0^A(t_m,t_n') + \Delta\bar{t}\sum_{i=m}^{n} w_i K^A(t_m,\bar{t}_i)G^A(\bar{t}_i,t_n'),\\
G^A(t_m,t_n') &\approx G_0^A(t_m,t_n') + \Delta\bar{t}\sum_{i=m+1}^{n} w_i K^A(t_m,\bar{t}_i)G^A(\bar{t}_i,t_n'),
\end{aligned} \tag{A14}$$

where $K^A(t_m,t_m)=0$ is used. In the equation for G^A it is not possible to gradually propagate in the direction of time since $G^A(t_m,t'_n)$ depends on later times $m=m+1,\ldots,n$; for a fixed time t'_n, in other words, this equation is not of the Volterra type [57] where the causal structure is evident from the limits of the integral. To get a Volterra type of equation for G^A we have to use another form of the CPT equation:

$$\hat{G}=\hat{G}_0+\hat{G}\bullet\hat{V}\bullet\hat{G}_0, \tag{A15}$$

where now $\hat{K}=\hat{V}\bullet\hat{G}_0$. Proceeding in the same way as above we derive the following equation in discretized time for the advanced Green's function:

$$G^A(t_m,t'_n)\approx G_0^A(t_m,t'_n)+\Delta\bar{t}\sum_{i=m+1}^{n-1}w_iG^A(t_m,\bar{t}_i)K^A(\bar{t}_i,t'_n). \tag{A16}$$

We now can gradually proceed in the second index t'_n for a fixed t_m.

Similarly, for the retarded Green's function we get

$$G^R(t_{m1},t'_{m2})\approx G_0^A(t_{m1},t'_{m2})+\Delta\bar{t}\sum_{i=m2+1}^{m1-1}w_iK^R(t_{m1},\bar{t}_i)G^R(\bar{t}_i,t'_{m2}), \tag{A17}$$

where we can progress in time by incrementing t_{m1} for a fixed t'_{m2}.

For the mixed Green's function, if we use the CPT Eq. (A15), we obtain the following integral equation:

$$G^{\ulcorner}(\tau,t)\approx G_0^{\ulcorner}(\tau,t)+\int_0^{t'}K^{\ulcorner}(\tau,\bar{t})G^A(\bar{t},t)d\bar{t}+\int_0^{-i\beta}K^M(\tau,\bar{\tau})G^{\ulcorner}(\bar{\tau},t)d\bar{\tau}. \tag{A18}$$

Since in the convolution including $G^{\ulcorner}$ the integration over τ is on the whole Matsubara branch, it is not possible to gradually proceed in time. So the way out is to choose the other CPT Eq. (A15) to end up in a Volterra-type equation:

$$G^{\ulcorner}(\tau_{m1},t_{m2})\approx G_0^{\ulcorner}(\tau_{m1},t_{m2})+\Delta t\sum_{i=0}^{m2-1}w_iG^{\ulcorner}(\tau_{m1},t_i)K^A(t_i,t_{m2})+\Delta\tau\sum_{i=0}^{N_M-1}w_iG^M(\tau_{m1},\tau_i)K^{\ulcorner}(\tau_i,t_{m2}). \tag{A19}$$

Here one can proceed in t_{m2} for a fixed τ_{m1}. The full information of the Matsubara Green's function on the imaginary axis is necessary to calculate the mixing Green's function. This can be done by equilibrium techniques; see Appendix B.

Finally, for the lesser Green's function we have

$$G^<(t_{m1},t_{m2})\approx G_0^<(t_{m1},t_{m2})+\Delta t\sum_{i=0}^{m2-1}w_iK^<(t_{m1},t_i)G^A(t_i,t_{m2})+\Delta\tau\sum_{i=0}^{N_M-1}w_iK^{\urcorner}(t_{m1},\tau_i)G^{\ulcorner}(\tau_i,t_{m2})+\Delta t\sum_{i=0}^{m1-1}w_iK^R(t_{m1},t_i)G^<(t_i,t_{m2}). \tag{A20}$$

APPENDIX B: CALCULATING EQUILIBRIUM GREEN'S FUNCTION G^M

The CPT equation for G^M is not of the Volterra type, so it is not possible to gradually proceed along the Matsubara axes. Fortunately, due to the time-translation invariance of the Green's function, G^M only depends on the time difference and so one can use Fourier transformation to go over to the frequency representation. In this way one still has to do the inversion process to get CPT Green's function but in this way the dimension reduces to the size of the lattice.

The Fourier transformations between the Green's functions are as follows:

$$G(\tau)=\frac{1}{\beta}\sum_{n=-\infty}^{\infty}G(i\omega_n)e^{-i\omega_n\tau},$$
$$G(i\omega_n)=\int_0^{\beta}d\tau e^{i\omega_n\tau}G(\tau), \tag{B1}$$

where $\tau\in[0,\beta]$. By using a fast Fourier transformation (FFTW), the above transformation can be carried out efficiently. When doing the inverse transformation we truncate the number of Matsubara frequencies. By using N points equally distributed among positive and negative frequencies we get the approximation

$$G(\tau)\approx\frac{1}{\beta}\sum_{n=-N/2}^{N/2-1}G(i\omega_n)e^{-i\omega_n\tau}=\mathrm{DIFT}[G(i\omega_n)],$$
$$\omega_n=\frac{\pi}{\beta}2n, \tag{B2}$$

where DIFT stands for discrete inverse Fourier transformation. This scheme poorly describes $G(\tau)$ due to missing contributions from the tail of $G(i\omega)$ ($\omega_n\to\infty$). In practice, it is not possible to consider an infinite number of frequencies so one should calculate the tail correction directly. If we look at the asymptotic behavior ($\omega_n\to\infty$) for the noninteracting Green's function we realize

$$G(i\omega_n)\sim-\frac{i}{\omega_n}. \tag{B3}$$

The asymptotic tail of $G_A(\tau)$ can be readily calculated by doing the Fourier transformation. For bosons we get:

$$G_A(\tau)=-\frac{2}{\beta}\sum_{n=0}^{\infty}\frac{\sin(\omega_n\tau)}{\omega_n}=-\frac{1}{2}+\frac{\tau}{\beta}. \tag{B4}$$

After a little algebra we can collect all contributions at high imaginary frequencies in the tail of the Green's function $G_T(\tau)$ and write

$$G(\tau)=\mathrm{DIFT}[G(i\omega_n)]+G_T(\tau),$$
$$G_T(\tau)=-\frac{1}{2}+\frac{\tau}{\beta}+\frac{2\pi}{\beta}\sum_{n=0}^{N/2-1}\frac{\sin(\omega_n\tau)}{\omega_n}. \tag{B5}$$

[1] I. Bloch, J. Dalibard, and W. Zwerger, Rev. Mod. Phys. **80**, 885 (2008).

[2] M. Lewenstein, A. Sanpera, and V. Ahufinger, *Ultracold Atoms in Optical Lattices Simulating Quantum Many-Body Systems* (Oxford University Press, Oxford, 2012).

[3] N. Strohmaier, D. Greif, R. Jördens, L. Tarruell, H. Moritz, T. Esslinger, R. Sensarma, D. Pekker, E. Altman, and E. Demler, Phys. Rev. Lett. **104**, 080401 (2010).

[4] S. Sachdev, *Quantum Phase Transitions* (Cambridge University Press, Cambridge, 1999).

[5] S. Suzuki, J.-i. Inoue, and B. K. Chkarabarti, *Quantum Ising Phases and Transitions in Transverse Ising Models*, Lecture Notes in Physics Vol. 862 (Springer-Verlag, Berlin, Heidelberg, 2013).

[6] F. Meinert, M. J. Mark, E. Kirilov, K. Lauber, P. Weinmann, A. J. Daley, and H.-C. Nägerl, Phys. Rev. Lett. **111**, 053003 (2013).

[7] D. Rossini, A. Silva, G. Mussardo, and G. E. Santoro, Phys. Rev. Lett. **102**, 127204 (2009).

[8] P. Calabrese, F. H. L. Essler, and M. Fagotti, Phys. Rev. Lett. **106**, 227203 (2011).

[9] R. Kubo, J. Phys. Soc. Jpn. **12**, 570 (1957).

[10] J. Schwinger, J. Math. Phys. **2**, 407 (1961).

[11] L. P. Kadanoff and G. Baym, *Quantum Statistical Mechanics* (Benjamin, New York, 1962).

[12] L. V. Keldysh, Sov. Phys. JETP **20**, 1018 (1965).

[13] M. Wagner, Phys. Rev. B **44**, 6104 (1991).

[14] J. K. Freericks, V. M. Turkowski, and V. Zlatic, Phys. Rev. Lett. **97**, 266408 (2006).

[15] P. Schmidt and H. Monien, arXiv:cond-mat/0202046.

[16] F. Hofmann, M. Eckstein, E. Arrigoni, and M. Potthoff, Phys. Rev. B **88**, 165124 (2013).

[17] C. Jung, A. Lieder, S. Brener, H. Hafermann, B. Baxevanis, A. Chudnovskiy, A. N. Rubtsov, M. I. Katsnelson, and A. I. Lichtenstein, Ann. Phys. **524**, 49 (2012).

[18] M. Knap, W. von der Linden, and E. Arrigoni, Phys. Rev. B **84**, 115145 (2011).

[19] H. Aoki and N. Tsuji, Rev. Mod. Phys. **86**, 779 (2014).

[20] K. Balzer and M. Eckstein, Phys. Rev. B **89**, 035148 (2014).

[21] M. Balzer and M. Potthoff, Phys. Rev. B **83**, 195132 (2011).

[22] C. Gramsch and M. Potthoff, Phys. Rev. B **92**, 235135 (2015).

[23] E. Arrigoni, M. Knap, and W. von der Linden, Phys. Rev. Lett. **110**, 086403 (2013).

[24] A. Dorda, M. Nuss, W. von der Linden, and E. Arrigoni, Phys. Rev. B **89**, 165105 (2014).

[25] A. Dorda, M. Ganahl, H. G. Evertz, W. von der Linden, and E. Arrigoni, Phys. Rev. B **92**, 125145 (2015).

[26] D. D. Sénéchal, D. Perez, and M. Pioro-Ladrière, Phys. Rev. Lett. **84**, 522 (2000).

[27] C. Gros and R. Valentí, Phys. Rev. B **48**, 418 (1993).

[28] P. Danielewicz, Ann. Phys. (NY) **152**, 239 (1984).

[29] J. Rammer and H. Smith, Rev. Mod. Phys. **58**, 323 (1986).

[30] E. Lieb, T. Schultz, and D. Mattis, Ann. Phys. (NY) **16**, 407 (1961).

[31] P. Pfeuty, Ann. Phys. (NY) **57**, 79 (1970).

[32] O. Derzhko, J. Phys. Stud. (L'viv) **5**, 49 (2001).

[33] M. Potthoff, Eur. Phys. J. B **32**, 429 (2003).

[34] M. Potthoff, Eur. Phys. J. B **36**, 335 (2003).

[35] W. Koller and N. Dupuis, J. Phys.: Condens. Matter **18**, 9525 (2006).

[36] M. Aichhorn, E. Arrigoni, M. Potthoff, and W. Hanke, Phys. Rev. B **74**, 235117 (2006).

[37] M. G. Zacher, R. Eder, E. Arrigoni, and W. Hanke, Phys. Rev. B **65**, 045109 (2002).

[38] W. Metzner, Phys. Rev. B **43**, 8549 (1991).

[39] S. Pairlaut, D. Sénéchal, and A. M. S. Tremblay, Eur. Phys. J. B **16**, 85 (2000).

[40] H. Hafermann, S. Brener, A. N. Rubstov, M. I. Katsnelson, and A. I. Lichtenstein, JETP Lett. **86**, 677 (2007).

[41] D. D. Sénéchal, D. Perez, and D. Plouffe, Phys. Rev. B **66**, 075129 (2002).

[42] M. Bonitz, *Progress in Nonequilibrium Green's Functions IV* (World Scientific, Singapore, 2000).

[43] M. T. Tran, Phys. Rev. B **78**, 125103 (2008).

[44] E. Arrigoni, M. Knap, and W. von der Linden, Phys. Rev. B **84**, 014535 (2011).

[45] M. Knap, E. Arrigoni, and W. von der Linden, Phys. Rev. B **83**, 134507 (2011).

[46] D. C. Langreth, in *Linear and Nonlinear Electron Transport in Solids*, edited by J. T. Devreese and V. E. van Doren (Plenum Press, New York and London, 1976).

[47] Z. Friedman, Phys. Rev. B **17**, 1429 (1978).

[48] R. J. Elliott and C. Wood, J. Phys. C: Solid State Phys. **4**, 2359 (1971).

[49] J. Oitmaa and M. Plischke, J. Phys. C: Solid State Phys. **9**, 2093 (1976).

[50] A. J. Daley, C. Kollath, U. Schollwöck, and G. Vidal, J. Stat. Mech. (2004) P04005.

[51] S. R. White and A. E. Feiguin, Phys. Rev. Lett. **93**, 076401 (2004).

[52] M. C. Banuls, M. B. Hastings, F. Verstraete, and J. I. Cirac, Phys. Rev. Lett. **102**, 240603 (2009).

[53] D. Gobert, C. Kollath, U. Schollwöck, and G. Schuetz, Phys. Rev. E **71**, 036102 (2005).

[54] J. Ren, Y. Z. Wu, and S. Zhu, Int. J. Theor. Phys. **52**, 3167 (2013).

[55] T. Sabetta and G. Misguich, Phys. Rev. B **88**, 245114 (2013).

[56] J. Ren, Y. Z. Wu, and X. F. Xu, Sci. Rep. **5**, 14743 (2015).

[57] H. Brunner and P. J. van der Houwen, *The Numerical Solution of Volterra Equations*, CWI Monographs, Vol. 3 (North-Holland, Amsterdam, 1986).